Polymer 49 (2008) 4369–4377

Contents lists available at ScienceDirect

Polymer

journal homepage: www.elsevier.com/locate/polymer

Novel photoluminescent polymers containing fluorene and 2,4,6-triphenyl pyridine moieties: Effects of noncoplanar molecular architecture on the electro-optical properties of parent matrix

Hong-Ji Jiang [a], Zhi-Qiang Gao [a], Feng Liu [b], Qi-Dan Ling [a], Wei Wei [b], Wei Huang [a,*]

[a] Jiangsu Key Laboratory for Organic Electronics & Information Displays, Institute of Advanced Materials, Nanjing University of Posts & Telecommunications, 9 Wenyuan Road, Nanjing 210046, China
[b] Institute of Advanced Materials, Fudan University, 220 Handan Road, Shanghai 200433, China

ARTICLE INFO

Article history:
Received 7 April 2008
Received in revised form 27 June 2008
Accepted 5 July 2008
Available online 22 July 2008

Keywords:
Polymer light-emitting diodes
Synthesis
Electro-optical

ABSTRACT

In order to investigate the electro-optical property variations among the target topology-varied polymers with diverse molecular architectures, a series of polymers (**P0**–**P2**), having sterically hindered side chains, based on fluorene and pyridine derivatives were successfully synthesized *via* simple synthetic route and fully characterized *via* various spectroscopic methods and cyclic voltammetry measurements. The experiments demonstrate that all polymers with almost equivalent absorption and photoluminescence emission properties take on a wide band gap with blue emission in THF solution and thin solid film. However, their energy levels derived from the onset of electrochemical potential in thin solid films exhibit significant differences, which are considered to be due to the branched molecular frameworks on the basis of theoretical calculations. It is demonstrated that the electro-optical properties of wide band gap rigid noncoplanar copolymers are tunable by the sterically hindered pyridine moieties, and these experiments can serve as an excellent exploratory example for fine band gap and photophysics control principle in the p–n heterostructure polymers through the partial planarization of the π-system.

1. Introduction

Highly soluble fluorene-based conjugated polymers are considered as an outstanding class of blue light-emitting materials due to their good thermal stability, high hole mobility, easy processability and high photoluminescence (PL) quantum yield in thin solid films. During the past decade, a variety of copolymers derived from 2,7-fluorenes and the comonomers that contain delocalized π-electrons has been actively investigated, and the development of such copolymers has led to the preparation of a series of fluorene-containing copolymers for polymeric light-emitting diodes (PLEDs) with color spanning the entire visible range [1,2]. However, the most intensely studied polymers are mainly linear conjugated π-systems, which tend to aggregate and end up with self-quenching of their luminescence, while their branched counterparts with different molecular architectures are still rare now, and the hyperbranched approach has been generally regarded as an effective method for the design of amorphous optoelectronic materials [3–10]. One of the major advantages of polyfluorene (**PF**) derivatives is that their electronic properties can be tuned *via* the modification of the comonomer block. The fluorene homopolymer has a large band gap (3.6 eV), thus, the emission color of **PF** copolymers can be tuned over the whole visible region by introducing small band gap comonomers into the polymer backbone [11–19]. It is believed that most of these materials for electro-optical applications will benefit from a full understanding of the dependence of charge-transport properties on the morphology of thin solid films and the electronic structure of the molecular chain. However, only a limited number of fluorene-based copolymers are known to exhibit deep-blue electroluminescence. It is believed that the partial planarization of the π-system in the aromatic fluorene repeat units is more effective for an emission in the blue region of the electromagnetic spectrum than that of parent **PF** [20,21].

The electro-optical properties of conjugated polymers are originated from the limited numbers of states between their lowest unoccupied molecular orbital (LUMO) and highest occupied molecular orbital (HOMO) energy levels, and their energy band gaps (E_g) depend on their conjugation lengths [22]. One effective way to tune E_g of conjugated polymers is to alternate electron-donors and electron-acceptors in the polymer main chains [23]. This can be achieved by incorporating electron-accepting subunits with large atomic orbital coefficients at the coupling position. The

* Corresponding author. Tel.: +216548 5675; fax: +216565 5123.
E-mail address: wei-huang@njupt.edu.cn (W. Huang).

0032-3861/$ – see front matter © 2008 Elsevier Ltd. All rights reserved.
doi:10.1016/j.polymer.2008.07.023

simplest molecular structure to fulfill this requirement is a pyridine ring containing electron-deficient imine nitrogen [24]. To the best of our knowledge, since they can harvest both singlet and triplet excitons, enabling internal quantum efficiencies close to 100%, the attention in most reports about the pyridine building block in organic light-emitting diodes (OLEDs) application has been predominantly paid to the electrophosphorescent metal complexes [25], whereas there are few reports about **PF** containing pyridine moiety with branched molecular architecture as yet. In comparison to a benzene ring, pyridine is an electron-deficient aromatic heterocycle, with a localized lone pair of electrons in sp^2 orbital on the nitrogen atom. Thus, the polymers containing pyridine moiety have an increased electron affinity and improved electron-transporting properties, while still possessing the possibility of protonation or alkylation of the lone pair electrons as a way of modifying their properties. It seems that the chromogenic phenomena can be produced by a delicate balance between the steric hindrance created by the side pendants along the backbone and the attractive molecular interactions through alternating approaches. Such molecular structure design may combine the desirable properties of both dendrimer and pyridine units into **PF**. In this regard, by using pyridine derivatives to alter the chemical structures, control the conjugation length and alter the packing of the polymer chains in the solid phase, one can finely tune the electro-optical properties through this alternating copolymer design.

Herein as an extension of our efforts to organic conjugated materials with a partial planarization of the π-system by p–n alternating concept, we firstly present the synthesis and characterization of a series of novel thermally stable polymers (Scheme 1 – **P0**–**P2**) based on fluorene and 2,4,6-triphenylpyridine derivatives *via* Pd(0)-catalyzed Suzuki coupling reaction. We intend to introduce the pyridine derivatives as pendants into linear **PF** to correlate the electro-optical properties with the zigzag molecular structures of polymers. Through experimental and theoretical studies, some interesting results related with the molecular topology are obtained and discussed. It is found that these pyridine systems can serve as excellent examples of the band gap and photophysics control principle in the p–n heterostructure polymers with a partial planarization of the π-system.

2. Experimental

2.1. Materials and instruments

Fluorene, *n*-butyl-lithium, 2,7-dibromo-fluorene, 2-bromo-fluorene, 4-bromobenzaldehyde, 1-(4-bromophenyl)ethanone, acetophenone, tri-isopropyl borate and tetrakis(triphenylphosphine)palladium(0) ($Pd(PPh_3)_4$) were purchased from Acros Organics and used without further purification. Tetrahydrofuran (THF) and toluene were distilled over sodium/benzophenone under nitrogen atmosphere. The other common solvents were purified according to the standard methods.

All NMR spectra were recorded on a Varian Mercury plus 400 at 22 °C. Tetramethylsilane was used as internal reference for all the compounds. Gel permeation chromatography (GPC) results were obtained by using Shimadzu LC-VP system with polystyrenes as the standard and THF as the eluent. Thermogravimetric analysis (TGA) and differential scanning calorimetry (DSC) scans were done on Shimadzu DTG-60A and DSC-60A equipments with a heating rate of 10 °C/min and nitrogen as the purge gas, respectively. Elemental analysis was performed on a CHNS-O (Elementar Co.). The UV–vis absorption and PL emission spectra were recorded on Shimadzu UV-3150 and RF-5300PC spectrometers, respectively. The molecular masses of intermediates were determined by Shimadzu Matrix assistant laser desorption/ionization time-of-flight mass spectrometry (MALDI-TOF MASS). Cyclic voltammetry (CV) was performed on an Autolab Pgstat30 potentiostat/galvanostat system (Ecochemie, Netherlands). The experiments were carried out on glass carbon electrode in acetonitrile solution containing 0.1 M tetrabutylammonium hexafluorophospate ($TBAPF_6$) using a Pt wire as counter electrode and an $Ag/AgNO_3$ (0.1 M) electrode as reference electrode at a scan rate of 100 mV/s at room temperature.

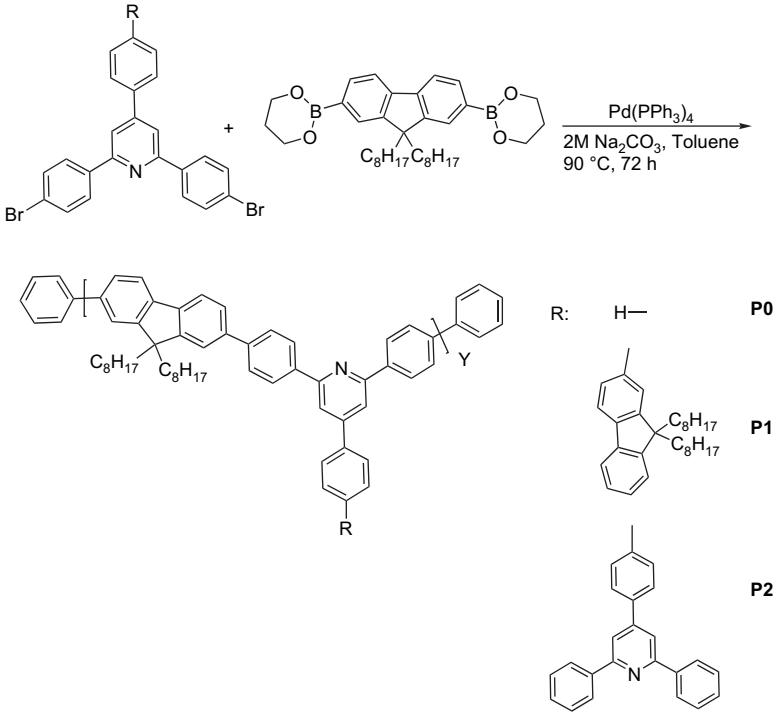

Scheme 1. The synthetic route of polymers **P0**–**P2**.

2.2. Preparation of the monomers

The monomers of 2,7-bis(trimethylene boronate)-9,9-dioctylfluorene (**M0**), 2,6-bis(4-bromophenyl)-4-phenyl pyridine (**M1**), 2,6-bis(4-bromophenyl)-4-(4-(9,9-dioctyl-fluoren)phenyl)pyridine (**M2**) and **M3** were synthesized according to documented procedures (Scheme 2) [26–28].

2.3. Synthesis of 2,7-bis(trimethylene boronate)-9,9-dioctylfluorene (*M0*)

Into the solution of 2,7-dibromo-9,9-dioctylfluorene (5.05 g, 9.22 mmol) in anhydrous THF (50 mL), *n*-butyl-lithium (19.5 mL, 31.2 mmol) was added dropwise at −78 °C for 30 min. The reaction mixture was stirred at −78 °C for 2 h before tri-isopropyl borate (8.3 mL, 35.75 mmol) was added in one portion. The reaction was slowly heated to room temperature, stirred overnight and then was poured into crushed ice containing 2 M HCl aqueous solution while being well stirred. The reaction was extracted with ether and the combined extracts were evaporated to give a white solid of 9,9-dioctylfluorene-2,7-diboronic acid. Then diboronic acid was refluxed with propane-1,3-diol (1.6 mL, 22.13 mmol) in 30 mL toluene for 10 h. After the routine workup, the crude product was purified with column chromatography on silica gel with petroleum ether/ethyl acetate (4:1) as the eluent to afford **M0** (3.45 g, 6.18 mmol) as white crystals in a yield of 68.4%. ^{1}H NMR (400 MHz, $CDCl_3$): δ 0.54 (m, 4H), 0.80 (m, 6H), 0.91–1.21 (m, 12H), 1.98 (m, 8H), 2.01–2.08 (m, 4H), 4.15–4.22 (m, 8H), 7.59–7.77 (m, 6H). ^{13}C NMR (400 MHz, $CDCl_3$): δ 14.301, 22.815, 23.897, 27.677, 29.460, 30.245, 32.036, 34.208, 36.228, 40.732, 55.104, 62.237, 119.385, 127.958, 132.546, 142.082, 150.520.

2.4. Synthesis of 2,6-bis(4-bromophenyl)-4-phenylpyridine (*M1*)

A flask charged with a mixture of benzaldehyde (2.67 g, 25.1 mmol), 4-bromoacetophenone (4.98 g, 25.1 mmol) and 2% aqueous sodium hydroxide (75 mL) was vigorously stirred at room temperature for 30 min, followed by being heated at 60 °C for 10 h. After the completion of the reaction monitored by TLC, it was cooled to room temperature, and the precipitated light yellow solid was filtered, washed thoroughly with water, air-dried to give 1,3-bis(4-bromophenyl)-propenone (8.36 g, 2.28 mmol) in a yield of 91%. 4-Bromoacetophenone (2.0 g, 10.04 mmol), 1,3-bis(4-bromophenyl)-propenone (3.68 g, 10.04 mmol) and powder sodium hydroxide (0.8 g, 20.08 mmol) were crashed together with a pestle and mortar for 2 h and then the yellow powder was added to a stirred solution of ammonium acetate (6.8 g, excess) in ethanol (68 mL). The reaction mixture was heated to reflux for 10 h. Upon cooling to room temperature, a precipitate was filtered, washed with water three times and dried to afford the product. It was purified by column chromatography on silica gel eluting with petroleum ether/chloroform (3:1) to give a white solid of **M1** (3 g, 5.51 mmol) in a yield of 50%. ^{1}H NMR (400 MHz, $CDCl_3$): δ 7.434–7.602 (m, 3H), 7.602–7.698 (m, 4H), 7.699–7.792 (m, 2H), 7.831–7.928 (s, 2H), 8.002–8.122 (s, 4H). ^{13}C NMR (400 MHz, $CDCl_3$): δ 117.438, 123.919, 127.423, 128.908, 129.450, 129.466, 132.130, 138.430, 138.81, 150.91, 156.61. MS (MALDI-TOF) Calcd for $C_{23}H_{14}Br_3N$ m/z (%) = 465.18 (100.0); found m/z (%) = 465.60 (100.0). ($C_{23}H_{15}Br_2N$) (465.2) Calcd. C, 59.38; H, 3.25; N, 3.01. Found C, 59.51; H, 3.14; N, 3.12.

2.5. Synthesis of 2,6-bis(4-bromophenyl)-4-(4-(9,9-dioctyl-fluoren)phenyl)pyridine (*M2*) and *M3*

M2 and **M3** were synthesized similarly according to procedure to prepare **M1**.

2.5.1. Monomer *M2*

Total yield: 40%. ^{1}H NMR (400 MHz, $CDCl_3$): δ 0.42–0.87 (m, 10H), 0.97–1.24 (m, 20H), 1.87–2.17 (m, 4H), 7.30–7.42 (m, 3H), 7.57–7.70 (m, 6H), 7.72–7.90 (m, 6H), 7.91–7.99 (s, 2H), 8.00–8.19 (m, 4H). ^{13}C NMR (400 MHz, $CDCl_3$): δ 14.240, 22.760, 29.365, 30.150, 31.915, 33.630, 35.510, 40.515, 55.378, 117.114, 120.172, 121.640, 123.846, 126.18, 126.571, 128.380, 128.890, 129.460, 132.190, 136.040, 137.370, 138.480, 139.057, 140.770, 141.263, 141.293, 150.429, 150.767, 151.271, 151.848, 156.453, 156.711. MS (MALDI-TOF) Calcd. m/z (%) = 853.81 (100.0); found m/z (%) = 853.90 (100.0). ($C_{52}H_{55}Br_2N$) (853.8) Calcd. C, 73.15; H, 6.49; N, 1.64. Found C, 73.28; H, 6.38; N, 1.59.

2.5.2. Monomer *M3*

Total yield: 30%. ^{1}H NMR (400 MHz, $CDCl_3$): δ 7.380–7.724 (m, 10H), 7.764–8.013 (m, 12H), 8.013–8.153 (m, 4H), 8.155–8.360 (m, 4H). ^{13}C NMR (400 MHz, $CDCl_3$): δ 117.167, 123.909, 127.340, 127.430, 128.095, 128.989, 129.227, 132.158, 138.572, 139.787, 149.768, 150.170, 156.772, 157.99. MS (MALDI-TOF) Calcd. m/z (%) = 768.08 (100.0); found m/z (%) = 768.90 (100.0). ($C_{46}H_{30}Br_2N_2$) (768.08) Calcd. C, 71.70; H, 3.92; N, 3.64. Found C, 71.62; H, 3.84; N, 3.71.

2.6. Synthesis of poly((2,7-diyl-9,9-dioctylfluorene)-co-(2,6-bis(4-phenyl)-4-phenylpyridine)) (*P0*)

All of the polymerizations were carried out by palladium(0)-catalyzed Suzuki coupling reactions with equivalently molar ratio of the diboronic ester monomer to the dibromo monomers under dry nitrogen protection. A typical procedure for the polymerization of the alternating copolymer **P0** is given below.

A mixture of **M0** (0.77 g, 1.37 mmol), **M1** (0.64 g, 1.37 mmol), alq336 and catalytic amount of $Pd(PPh_3)_4$ were added to a degassed mixture of toluene (20 mL) and Na_2CO_3 aqueous solution (2.0 M, 4.0 mL). The mixture was vigorously stirred at 90 °C for 72 h under nitrogen atmosphere. After the routine Suzuki end-capping reaction of 1-bromobenzene and phenyl boronic acid in turn, 50 mL toluene was added, and the organic layer was separated and washed with brine for drying over anhydrous $MgSO_4$. The residue was filtrated with a short column chromatography on silica gel with toluene as eluent to yield a light yellow solution. Upon part of solvent being evaporated off, the concentrated solution was dropped slowly into a solution of methanol while being well stirred. The obtained organic precipitate was collected on a filter, washed by methanol followed by soxhlet extraction with acetone for 48 h to remove the oligomers and catalyst residue. The recovered yield of the yellow solid was 70%. ^{1}H NMR (400 MHz, $CDCl_3$): δ 0.57–0.98 (br), 1.01–1.47 (br), 1.95–2.32 (br), 7.34–7.46 (br), 7.45–7.66 (br), 7.66–7.78 (br), 7.79–7.96 (br), 7.97–8.17 (br), 8.28–8.56 (br) (Fig. 1). $(C_{52}H_{57}N)_n$ $(695.45)_n$ Calcd. C, 89.73; H, 8.25; N, 2.01. Found C, 89.35; H, 8.42; N, 2.23.

2.7. Synthesis of poly((2,7-diyl-9,9-dioctylfluorene)-co-(2,6-bis(4-phenyl-4-(9,9-dioctyl-fluoren)phenyl)pyridine)) (*P1*) and *P2*

P1 and **P2** were synthesized similarly according to the procedure for preparing **P0**.

2.7.1. Polymer *P1*

M0 (0.77 g, 1.37 mmol), **M2** (1.17 g, 1.37 mmol), catalytic amount of $Pd(PPh_3)_4$, toluene (20 mL), alq336 and Na_2CO_3 aqueous solution (2.0 M, 4.0 mL) were used in the reaction mixture. ^{1}H NMR (400 MHz, $CDCl_3$): δ 0.61–0.95 (br), 1.02–1.48 (br), 1.93–2.25 (br), 7.31–7.46 (br), 7.45–7.79 (br), 7.66–7.79 (br), 7.79–8.01 (br), 8.01–8.18 (br), 8.22–8.31 (br), 8.31–8.56 (br) (Fig. 1). $(C_{81}H_{99}N)_n$

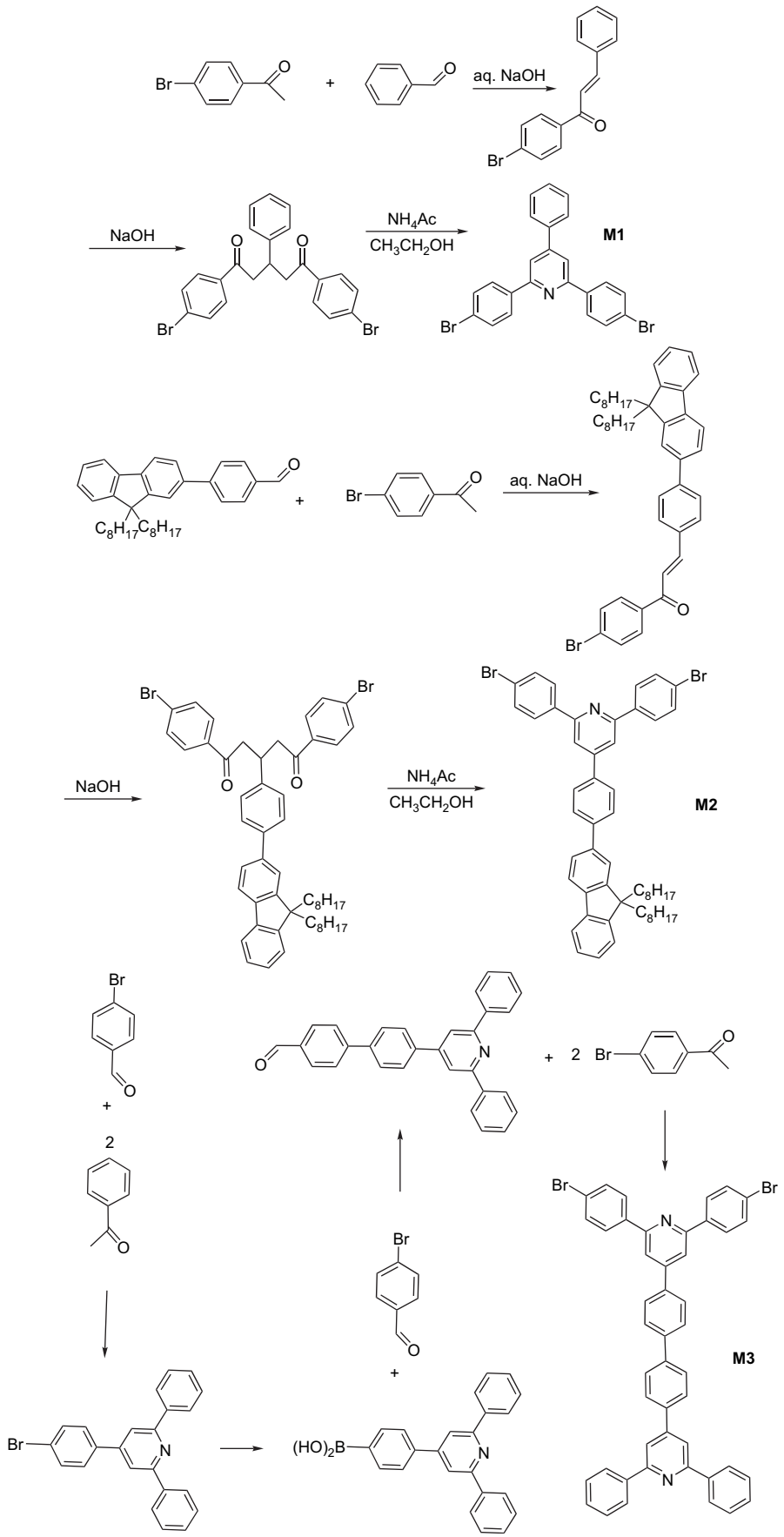

Scheme 2. The synthetic route of the target monomers.

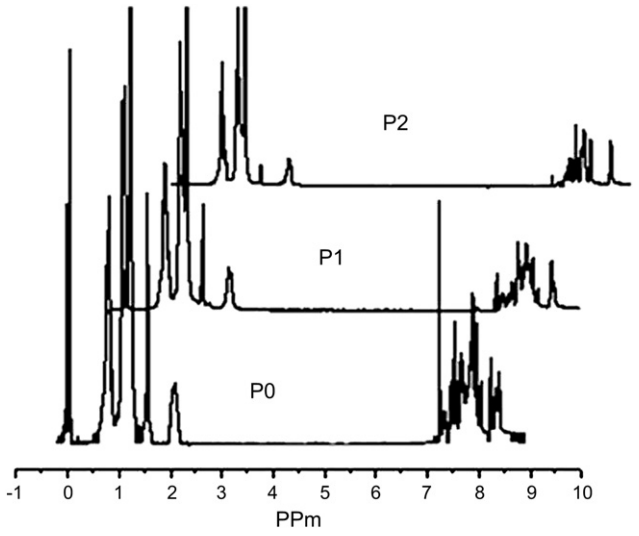

Fig. 1. ^{1}H NMR ($CDCl_3$, 400 MHz) shift spectra of polymers **P0**–**P2**.

$(1085.78)_n$ Calcd. C, 89.53; H, 9.18; N, 1.29. Found C, 89.25; H, 9.32; N, 1.37.

*2.7.2. Polymer **P2***

M0 (0.77 g, 1.37 mmol), **M3** (1.06 g, 1.37 mmol), catalytic amount of $Pd(PPh_3)_4$, toluene (20 mL), alq336 and Na_2CO_3 aqueous solution (2.0 M, 4.0 mL) were used in the reaction mixture. ^{1}H NMR (400 MHz, $CDCl_3$): δ 0.61–0.94 (br), 0.98–1.42 (br), 1.95–2.23 (br), 7.23–7.42 (br), 7.43–7.64 (br), 7.65–7.80 (br), 7.83–8.02 (br), 8.07–8.11 (br), 8.19–8.33 (br), 8.34–8.47 (br) (Fig. 1). $(C_{75}H_{72}N_2)_n$ $(1000.57)_n$ Calcd. C, 89.96; H, 7.25; N, 2.80. Found C, 89.52; H, 7.49; N, 2.95.

3. Results and discussion

3.1. Synthesis and characterization of the polymers

Polymers **P0**–**P2** were prepared *via* the Suzuki coupling method by using **M0**–**M2**, and **M3** at a feed ratio of 1:1 (Scheme 1). The synthetic route to the chosen new monomers of **M1**–**M3** is depicted in Scheme 2, according to a previously reported methodology through an alternative solid phase synthetic pathway of 4-bromobenzaldehyde, benzaldehyde, 1-(4-bromophenyl)ethanone and acetophenone derivatives with a relatively high yield [27]. The structures of resulting monomers and polymers have been well identified *via* ^{1}H NMR, ^{13}C NMR, GPC against standard polystyrene, elemental analysis and MALDI-TOF mass spectra, respectively. In addition, the elemental analysis results were consistent well with the calculated ones. All polymers were finally end-capped with benzene to improve their thermal and photophysical stabilities. **P0**–**P2** were completely soluble in common organic solvents, such as chloroform, toluene, ethyl acetate and so forth at room temperature. The weight-average molar mass (M_w) of **P0**–**P2** was 7700, 9900, and 11,800 with a polydispersity distribution index (PDI) of 1.42 (monomodal), 1.28 (monomodal) and 1.33 (monomodal), respectively (Table 2). We selected **P0** with lowest weight-average molar mass to investigate the thermal stability of these analogous polymers by using TGA and DSC under nitrogen atmosphere. The TGA results revealed that **P0** possessed a relatively excellent thermal stability with a decomposing temperature of 318 °C at 5% weight loss and a glass-transition temperature (T_g) of 62 °C. This T_g value can be attributed to the relatively low average molar mass of the polymer. The reasonably high thermal stability of the resulting polymer is expected to prevent the deformation of the polymer morphology and degradation of the polymer light emitting device by applied electric field of the OLEDs (Supplementary data). In addition, it is worth noticing that the dendronized copolymer **P0** is found to have higher T_g as compared with the reported **PF** ($T_g = 51$ °C) [29].

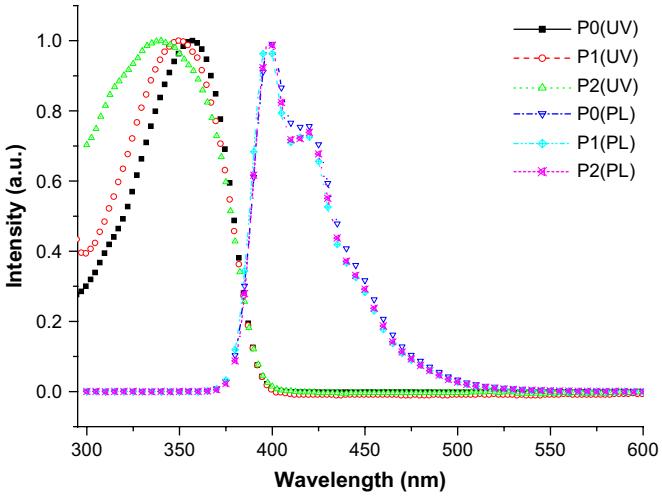

Fig. 2. Normalized UV–vis and PL emission spectra of polymers **P0**–**P2** in THF solution.

3.2. Photophysical properties

The photophysical properties of **P0**–**P2** were investigated in both dilute THF solutions and thin solid films. The absorption and PL emission data of the polymers are summarized in Figs. 2 and 3 and Table 1. As shown in Figs. 2 and 3, the absorption spectra of the polymer solutions and thin solid films are very similar with the peaks locating in the range from 340 to 357 nm, which can be attributed to the most prominent π–π^* transitions derived from the polymer backbones. The maximum absorption in solution undergoes a blue shift in the turn of **P0**–**P2**, indicating that the extra substituents on the side chain of pyridine rings have caused the gradual blue shifts of the π–π^* transitions from **P0** to **P2**. This suggests that the electron delocalization along the chain decreases as the comonomers change from **M1** to **M2** and **M3**. However, as

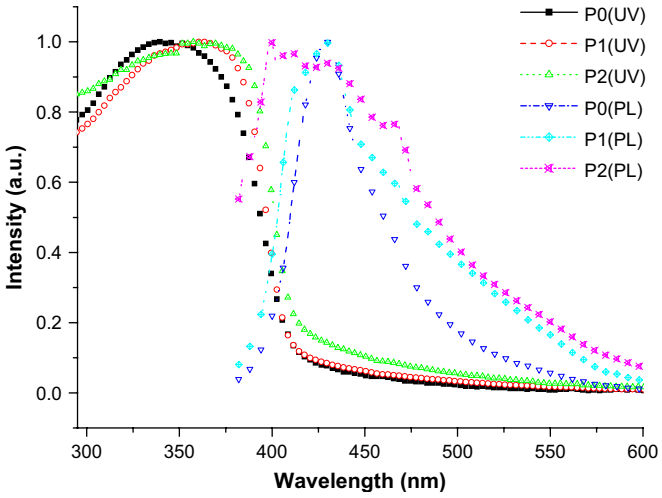

Fig. 3. Normalized UV–vis and PL emission spectra of polymers **P0**–**P2** in thin solid films.

Table 1
Absorption and PL emission spectral data of polymers in solution and thin solid films

Polymer	THF			Film		
	λ_{max}^{abs} [a] (nm)	$\lambda_{max}^{em/ex}$ [b] (nm)	E_g^{opt} [c] (eV)	λ_{max}^{abs} [a] (nm)	$\lambda_{max}^{em/ex}$ [b] (nm)	E_g^{opt} [c] (eV)
P0	357	398 (371)	3.15	342	428 (358)	3.04
P1	350	398 (367)	3.15	361	431 (359)	2.99
P2	340	398 (352)	3.15	357	399 (358)	3.01

[a] Maximum absorption wavelength.
[b] Maximum emission and excitation wavelength.
[c] Optical band gap determined from the UV–vis absorption onset.

calculated from the absorption onsets in THF solution, the optical band gaps of these polymers in solution are 3.15 eV, and the PL emission of **P0**–**P2** in THF solution exhibits a maximum blue emission of 398 nm invariantly. This indicates that the optical band gap and maximum absorption have been affected by the different features of the polymers and the PL emission band in solution is rarely associated with the size and number of the substituents, the resulted torsion angle and the relative movement of the phenyl rings [30].

Fig. 3 shows the UV–vis absorption and PL emission spectra of the polymers in thin solid films. Unlike that in THF solution, the maximum absorption of **P1** and **P2** in thin solid films exhibits a slight red shift relative to that of **P0**, while the maximum PL emission of **P1** and **P2** in thin solid films exhibits a small blue shift relative to that of **P0**, which can only be ascribed to the different congregating states in thin solid films. It is generally expected that the highly branched structure of **P1** and **P2** should make the molecule not easy to form a planar conjugated structure and the PL emission peaks of **P1** and **P2** in thin solid films should be blue shift relative to that of **P0**. The abnormal blue-shifted PL emission of **P1** and **P2** films shields light on the pronounced effects of fluorene and 2,4,6-triphenyl pyridine with bulky molecular size in the side chain of polymers to finely perturb the resulted torsion angle and the relative movement of the phenyl segments, which in turn tunes the general electro-optical properties of parent **PF** matrix in thin solid film. As can be seen from Fig. 3, the full width at half-maximum of the PL emission spectra in **P1** and **P2** thin solid films is larger than that of **P0**, it provides a key evidence that there is a higher probability for intra- as well as intermolecular interactions among the fluorophores when the fluorophore segment in the side groups is elongated, which in turn causes the broadening of the PL emission spectrum [31]. The PL emission spectra of the polymer solutions exhibit similar vibronic features with a narrow bandwidth and emission maxima at around 416–436 and 450–490 nm. In general, the presence of well-defined vibronic features in the emission spectra suggests that the polymer has a rigid and well-defined backbone structure [32,33]. All polymers of **P0**–**P2** exhibit two PL emissions in THF solution, and the emission peak is clearly not dependent upon the excitation wavelength. Here we try to give a preliminary explanation that there may exist a possible efficient energy transfer between the segments with different conjugated lengths. The similar emissions from these copolymers in comparison with that of **PF** homopolymer suggest that the pyridine derivatives in the polymer backbones do not prevent efficient energy transfer from the short conjugated emissions to the long ones in these copolymers [34,35].

Table 2
Polymerization results and molecular weights of polymers

Polymer	Yield (%)	M_n [a] ($\times 10^4$)	M_w [a] ($\times 10^4$)	PDI [b]
P0	70	0.49	0.77	1.42
P1	62	0.77	0.99	1.28
P2	60	0.89	1.18	1.33

[a] Molecular weight determined by GPC in THF based on polystyrene standards.
[b] Polydispersity distribution index.

Table 3
Electrochemical data of polymer thin solid films

Polymer	Reduction [a]	Oxidation [a]	LUMO/HOMO [c] (eV)	E_g^{cv} [d] (eV)	E_g^{opt} [e] (eV)
	E_{pa}/E_{pc} [b] (V)	E_{pc}/E_{pa} [b] (V)			
PF	−2.54/−2.80	1.78/0.87	−2.19/−5.82	3.63	2.78
P0	−2.66/−3.18	1.44/1.13	−2.02/−5.75	3.73	3.04
P1	−2.62/−3.20	1.48/1.20	−2.41/−5.85	3.44	2.99
P2	−2.43/−2.23	1.14/–	−2.39/−5.75	3.36	3.01

[a] Determined by cyclic voltammetry for polymer thin solid film coated on glassy carbon electrode.
[b] E_{pa} and E_{pc} stand for anodic peak potentials and cathodic peak potentials, respectively.
[c] HOMO and LUMO energy levels calculated with reference to ferrocene (4.7 eV).
[d] Electrochemical band gap obtained by cyclic voltammetry.
[e] Optical band gap determined from the UV–vis absorption onset in thin solid film.

3.3. Electrochemical properties

In order to find further information of conjugated structure for polymers, we employed CV to probe the HOMO and LUMO energy levels of **P0**–**P2** thin solid films. The HOMO and LUMO energy levels of thin solid films for **PF** end-capped with benzene were evaluated under same condition for comparison. The HOMO and LUMO energy levels of polymer thin solid films and the energy band gaps (E_g^{cv}) of the polymer thin solid films were calculated according to the following equations [36].

$$\text{LUMO} = -e(E_{red} + 4.71)(\text{eV}); \quad \text{HOMO} = -e(E_{ox} + 4.71)(\text{eV});$$
$$E_g^{cv} = e(E_{ox} - E_{red})(\text{eV})$$

The oxidation and reduction potentials derived from the onset of electrochemical potential are summarized in Table 3, and Figs. 4 and 5 illustrate the cyclic voltammogram curves in detail. Polymer **P2** exhibits an irreversible oxidation during the first CV scan, which is probably due to the irreversibility of one single two electron transfer or can be due to a much more negative potential for the second reduction step in unsymmetrical dipyridine blocks of **M3** unit [37]. No conclusive evidence is available for deciding between these two scenarios. The oxidized fluorene moieties in **P2** may feature a strong electron-accepting characteristic of **M3** segments and the conjugative coupling between **M3** and **P2** backbones

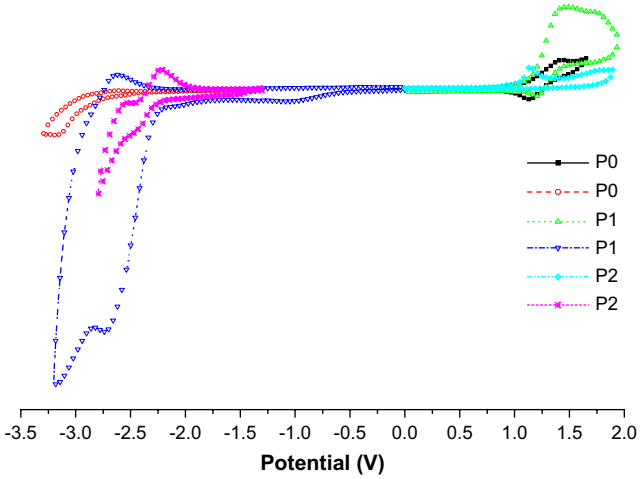

Fig. 4. Cyclic voltammogram curves of **P0**–**P2** thin solid films.

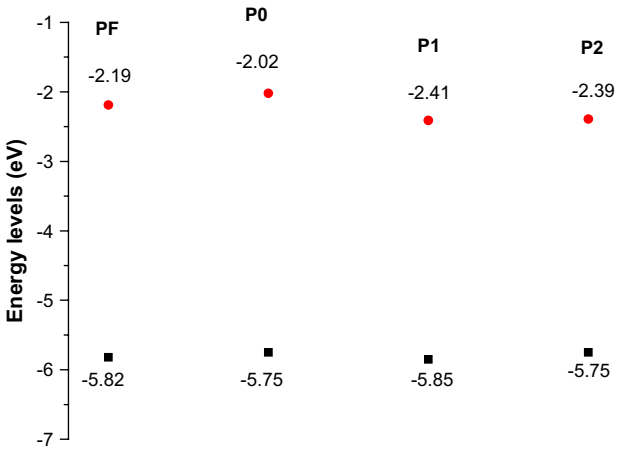

Fig. 5. The HOMO and LUMO energy levels of **PF**, **P0**–**P2** thin solid films.

dramatically lowers the chemical stability of intermediates [38]. Polymers **P0** and **P1** exhibit complete reversibility both in the p-doping and n-doping processes, suggesting the potential for bipolar charge-transport properties (see Fig. 4). In conjugated polymers, the maximum wavelengths of absorption and PL emission are determined by the band gap of material. The factors that influence the band gap of a polymer are conjugation length, solid-state intermolecular ordering and the presence of electron-withdrawing or -donating moieties. Therefore, by modifying one or more of these properties, polymers with controlled band gaps and thus, specific optical and electrical characteristics can be synthesized. The effective conjugation length, which is dependent upon the torsion angle between the repeating units along the polymer backbone, can be controlled by choosing sterically hindered units along the polymer backbone or by introducing bulky side chains to twist the units out of plane [39]. Generally, when electron-withdrawing substituents (such as bromine) are attached to the conjugated molecules, the electron density in the π-system of the conjugated molecule will be decreased. Consequently, the molecule will be stabilized and the oxidation potential will be increased in turn, corresponding to a shift of the HOMO energy level to lower energy. The HOMO and LUMO energy levels of **P0** are −5.75 and −2.02 eV, and the corresponding band gap is 3.73 eV. These values are considerably changed from those of **PF** [40], which validates that the zigzag fragments of 2,4,6-triphenylpyridine can greatly alter the energy levels of **PF** thin solid film and the introduction of V-shaped 2,4,6-triphenyl pyridine certainly distorts the linear conjugated structure of **PF** thin solid film. With the branched degree being further increased to **P1**, the reduction potential is considerably changed, which in turn makes the HOMO and LUMO energy levels of **P1** to be −5.85 and −2.41 eV. The LUMO energy level of **P1** thin solid film is decreased and the band gap is subsequently reduced to 3.44 eV. This indicates that the fluorene moiety in the side chain has perturbed the electronic unit and rendered the effective π-conjugation length of **P1** mainly located on **M2** segments. Similarly, when comparing the HOMO and LUMO energy levels of **P2** with those of **P0**, we can also find the same result that the triphenyl pyridine segments in the side chain of **P2** can lower the LUMO energy level, while keeping the HOMO energy level practically unchanged relative to that of **P0**. These results offer us a possible approach to finely tune the LUMO energy level of parent **PF** by grafting bulky segment to the main chain of polymer. In the turn of **PF**, **P1** and **P2**, the LUMO energy level is gradually lowered, which further validates that the π-electron-deficient pyridine substitutions in **M2** and **M3** enhance the electron injection capability of target materials [41]. In general, electron injection in conjugated electroluminescent polymers is much more difficult than hole injection, leading to the imbalance between the electron and hole injections from negative and positive contacts, respectively, and a shift of the recombination zone toward the region near the interface of the polymer/cathode. To overcome the difficulty, it is necessary for us to balance the injection/transport rates of opposite charges and decrease the barriers of charge injection from the opposite contacts. The lower LUMO/HOMO energy levels of **P1** relative to those of **P0** render it to be a potential electron-transporting/hole-blocking material, while **P2** can be used as an electron-transporting material [42]. All in all, through comparing the HOMO and LUMO energy levels of polymer thin solid films, it is distinctly indicated that the modulation of energy levels can be realized independently by grafting peripheral bulky pendants to the main chain of polymer, while keeping the absorption and PL emission properties of main chain approximatively unaffected. The interesting wide energy band gap and the good chelating capacity of the pyridine moiety for metal ions in these polymers will endow these analogs with the potential to be host for OLEDs [43] or as the sensitive optical probe [44]. Further analysis of the structures of polymers will allow us to clearly understand how the structure feature affects the electro-optical performance of conjugated material for device optimization. We are presently fabricating OLEDs or the sensitive optical biosensors that incorporate these molecules as active materials and will report our results in the due course.

3.4. Theoretical calculations

To provide further evidence for the photophysical properties of polymers, we have studied the geometries of repeating units of the polymers with the semiempirical Hartree–Fock Austin Model 1 (AM1) method in the Gaussian 03 program to reproduce the geometry of organic molecules in their ground state [45,46]. In this theoretical analysis, the starting unit cell geometries were taken from the central part of corresponding polymers, and the octyl segments of the molecules were simplified to be methyl units for their minor influence on the electro-optical properties of the zigzag molecules. A periodic one-dimensional system (**M-P0**, **M-P1**, and **M-P1** in Fig. 6) that involved as repeating units was employed as a model for polymers **P0**–**P2**. The molecular orbital contours of the HOMO and LUMO energy levels of the polymers are plotted in Fig. 6. We can see that the HOMO energy levels of all polymers mainly delocalize among the main chain of polymers, while the LUMO energy levels of **P1** and **P2** delocalize among the side chain of the molecule. The reduction (electron injection) starts at aromatic segments in the side chains of **P1** and **P2** [47,48], which further validates the vital role of **P1** and **P2** for electron-transporting. These values manifest that there is an obvious interaction between the pendants in the side chain and the main chain of the polymer, and the HOMO and LUMO energy levels of **P1** and **P2** can be modulated independently by grafting different moieties onto the main chain of polymers. As can be seen from Table 3, there exists obviously large difference between the optical band gap and the electrochemical band gap, which is owing to the different estimation basis. The optical band gap is calculated from the onset absorption, whereas the electrochemical band gap is estimated from the difference between onset oxidation and onset reduction potentials. Therefore, if the oxidation and reduction start from different segments, the estimated electrochemical band gap originated from the lower energy segment calculated from the onset absorption will be different from the optical band gap. It can also be found that the structural and configuration changes in the backbone cause an obvious variation in the energy band gaps of polymer thin solid films, while keeping the UV–vis absorption and

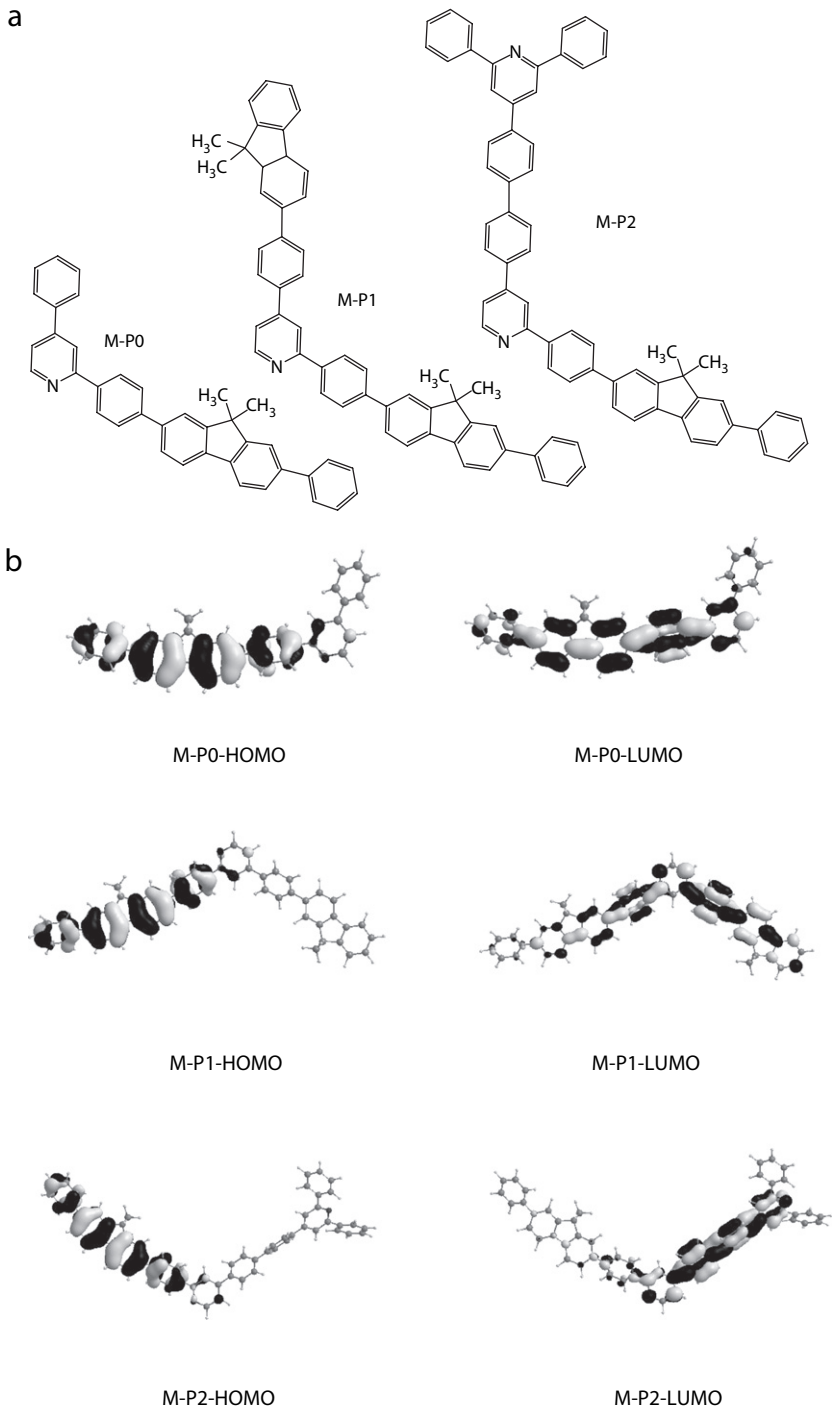

Fig. 6. The conceivable repeating conjugated segments: (a) the molecular orbital contours of HOMO and LUMO energy levels; (b) the repeating conjugated segments for polymers **P0**–**P2**.

PL emission properties of the polymers approximatively unchanged (Table 1).

4. Conclusions

In summary, a novel family of polymers based on fluorene and 2,4,6-triphenylpyridine derivatives was successfully synthesized and characterized *via* various spectroscopic methods and CV measurements. The influence of the zigzag structure on the electro-optical characteristics was further studied by using molecular orbital calculations. The experimental results demonstrate that all materials can provide wide band gap polymers with emission in the blue region. Although the absorption and PL emission behaviors of these polymers keep approximatively identical to each other, their energy levels derived from the onset of electrochemical potential in thin solid films exhibit some differences correlated, to a large extent, with the branched molecular frameworks. The observed electro-optical properties are consistent with theoretical calculations, and these systems can serve as excellent examples of the band gap control principle in the p–n heterostructure polymers with a partial planarization of the π-system. More importantly, this work has emphasized on the importance of chain structure

diversification and energy band gap design toward improved light-emitting materials in OLEDs.

Acknowledgments

This work was financially supported by the National Natural Science Foundation of China under Grants 20774043 and 20574012, the Natural Science Foundation of Jiangsu College Council KJD150148 and the Scientific Research Foundation of Nanjing University of Posts and Telecommunications under Grants NY206069.

Appendix. Supplementary data

Supplementary data associated with this article can be found in the online version, at doi:10.1016/j.polymer.2008.07.023.

References

[1] Wu CW, Tsai CM, Lin HC. Macromolecules 2006;39:4298–305.
[2] Chan LH, Lee YD, Chen CT. Macromolecules 2006;39:3262–9.
[3] Marsitzky D, Vestberg R, Blainey P, Tang BY, Hawker CJ, Carter KR. J Am Chem Soc 2001;123:6965–72.
[4] Pogantsch A, Wenzl FP, List EJW, Leising G, Grimsdale AC, Müllen K. Adv Mater 2002;14:1061–4.
[5] Bliznyuk VN, Carter SA, Scott JC, Klaerner G, Miller RD, Miller DC. Macromolecules 1999;32:361–9.
[6] Beaupre S, Ranger M, Leclerc M. Macromol Rapid Commun 2000;21:1013–8.
[7] Craig MR, Dekok MM, Hofstraat JW, Schenning APHJ, Meijer EW. J Mater Chem 2003;13:2861–2.
[8] Kulkarni P, Jenekhe SA. Macromolecules 2003;36:5285–96.
[9] Chochos CL, Tsolakis PK, Gregoriou VG, Kallitsis JK. Macromolecules 2004;37:2502–10.
[10] Surin M, Hennebicq E, Ego C, Marsitzky D, Grimsdale AC, Müllen K, et al. Chem Mater 2004;16:994–1001.
[11] Evans NR, Devi LS, Mak CSK, Watkins SE, Pascu SI, Kohler A, et al. J Am Chem Soc 2006;128:6647–56.
[12] Lee B, Yavuz MS, Sotzing GA. Macromolecules 2006;39:3118–24.
[13] Ego C, Marsitzky D, Becker S, Zhang J, Grimsdale AC, Müllen K, et al. J Am Chem Soc 2003;125:437–43.
[14] Kanibolotsky AL, Berridge R, Skabara PJ, Perepichka IF, Bradley DDC, Koeberg M. J Am Chem Soc 2004;126:13695–702.
[15] Hou Q, Zhou Q, Zhang Y, Yang W, Yang R, Cao Y. Macromolecules 2004;37:6299–305.
[16] Blondin P, Bouchard J, Beaupre S, Belletete M, Durocher G, Leclerc M. Macromolecules 2000;33:5874–9.
[17] Beaupre S, Leclerc M. Adv Funct Mater 2002;12:192–6.
[18] Zhang C, Choi S, Haliburton J, Cleveland T, Li R, Sun SS, et al. Macromolecules 2006;39:4317–26.
[19] Jung YK, Lee J, Lee SK, Cho HJ, Shim HK. J Polym Sci Part A Polym Chem 2006;44:4611–20.
[20] Yang CD, Scheiber H, List EJW, Jacob J, Müllen K. Macromolecules 2006;39:5213–21.
[21] Qi YH, Ding JF, Day M, Jiang J, Callender CL. Polymer 2006;47:8263–71.
[22] Yu WL, Meng H, Pei J, Huang W. J Am Chem Soc 1998;120:11808–9.
[23] Yu WL, Meng H, Pei J, Huang W, Li Y, Heeger AJ. Macromolecules 1998;31:4838–44.
[24] Pan XY, Liu SP, Chan HSO, Ng SC. Macromolecules 2005;38:7629–35.
[25] Zhen HY, Jiang CY, Yang W, Jiang JX, Huang F, Cao Y. Chem Eur J 2005;11:5007–16.
[26] Xin Y, Wen GA, Zeng WJ, Zhao L, Zhu XR, Fan QL, et al. Macromolecules 2005;38:6755–8.
[27] Yang JX, Tao XT, Yuan CX, Yan YX, Wang L, Liu Z, et al. J Am Chem Soc 2005;127:3278–9.
[28] Newkome GR, Shreiner CD. Polymer 2008;49:1–173.
[29] Ding JF, Day M, Robertson G, Roovers J. Macromolecules 2002;35:3474–83.
[30] Huang WY, Liaw BR, Chang MY, Han YK, Huang PT. Macromolecules 2007;40:8649–57.
[31] Mikroyannidis JA. Polymer 2000;41:8193–204.
[32] Teetsov J, Fox MA. J Mater Chem 1999;9:2117–22.
[33] Liaw DJ, Wang KL, Chang FC. Macromolecules 2007;40:3568–74.
[34] Peng Q, Peng JB, Kang ET, Neoh KG, Cao Y. Macromolecules 2005;38:7292–8.
[35] Cimrova V, Remmers M, Neher D, Wegner G. Adv Mater 1996;8:146–9.
[36] Hou JH, Tan ZA, He YJ, Yang CH, Li YF. Macromolecules 2006;39:4657–62.
[37] Gautrot JE, Hodge P. Polymer 2007;48:7065–77.
[38] Michinobu T, Okoshi K, Osako H, Kumazawa H, Shigehara K. Polymer 2008;49:192–9.
[39] Perzon E, Wang XJ, Admassie S, Inganäs O, Andersson MR. Polymer 2006;47:4261–8.
[40] Zhu R, Wen GA, Feng JC, Chen RF, Zhao L, Yao HP, et al. Macromol Rapid Commun 2005;26:1729–35.
[41] Wong KT, Hwu TY, Balaiah A, Chao TC, Fang FC, Lee CT, et al. Org Lett 2006;8:1415–8.
[42] Chen SH, Chen Y. J Polym Sci Part A Polym Chem 2004;42:5900–10.
[43] Chen YC, Huang GS, Hsiao CC, Chen SA. J Am Chem Soc 2006;128:8549–58.
[44] He F, Tang Y, Yu M, Feng F, An L, Sun H, et al. J Am Chem Soc 2006;128:6764–5.
[45] Jiang HJ, Wang HY, Feng JC, Wang CM, Fan QL, Wei W, et al. J Fluorine Chem 2006;127:973–6.
[46] Taranekar P, Abdulbaki M, Krishnamoorti R, Phanichphant S, Waenkaew P, Patton D, et al. Macromolecules 2006;39:3848–54.
[47] Yeh KM, Chen Y. J Polym Sci Part A Polym Chem 2006;44:5362–77.
[48] Roncali J. Macromol Rapid Commun 2007;28:1761–75.